Available online at www.sciencedirect.com
SCIENCE DIRECT®
Journal of Computational Physics 193 (2003) 226–242
JOURNAL OF COMPUTATIONAL PHYSICS
www.elsevier.com/locate/jcp

# TVD-interpolating matrix method prediction of flow with heat transfer

L. Hanich [a], M. Louaked [b,*]

[a] Applied Mathematics and Computing Group, School of Engineering, Cranfield University, UK
[b] Dept. de Mathématiques et Mécanique, Université de Caen, Campus II Bd. Maréchal Juin, Bât. Sciences, B P 5186, Caen Cedex 14032, France

Received 16 December 2002; received in revised form 28 July 2003; accepted 11 August 2003

**Abstract**

The use of the Interpolating Matrix Method to investigate the dynamical behaviour of natural convection flow will form the main focus of the work. We design an original and efficient numerical algorithm that mimic TVD constraints to rule out spurious overshoots and oscillations that appear near steep gradients, to solve fluid flow and heat transfer equations, and compare the results to some Benchmark numerical solutions.


*Keywords:* IMM; TVD; Flux limiters; Non-orthogonal grid; Heat flow

## 1. Introduction

For a number of years the natural convection problem has attracted numerical analysts because of the large practical applications such as crystal growth [13], solar energy collection [1], climatic conditioning of rooms [19] and many other technical fields as found in computers and nuclear reactors technologies [2,24]. Many numerical simulations have been associated to the investigation of this problem [4–6,14,20].

There are several basic approaches to solve partial differential equations on irregular region. Among these methods, The Interpolating Matrix Method (IMM). The IMM technique was first proposed by Koshizuka et al. [12] as a new generalized finite differences which requires no special treatment for curvilinear or non-uniform grids. The method is based on the Leith scheme to deal with the convective term in the Navier–Stokes equations. Unfortunately, the Leith scheme is a two-dimensionally unstable method arising from the interaction of two one-dimensional methods, each of which is stable. In our previous work

* Corresponding author. Tel.: +33-02-31-56-74-78; fax: +33-02-31-56-73-20.
*E-mail addresses:* l.hanich@cranfield.ac.uk (L. Hanich), louaked@meca.unicaen.fr (M. Louaked).

0021-9991/$ - see front matter 
doi:10.1016/j.jcp.2003.08.006

[18], we showed how to modify the method to get a stable and accurate TVD–IMM scheme. Different tools have been developed. Most importantly, three main features differentiate the two versions of the IMM. First, the stream–vorticity formulation is chosen and the IMM is adapted to it contrary to the use of primitive variables in the original IMM [12]. Furthermore, it is well known that, considering the storage and also the computational requirements, the stream function and vorticity formulation seems to be worthwhile. The pressure field can be obtained from the converged solutions. Second, The former technique contains no cross terms in the definition of the interpolation matrix which makes it less accurate in non-orthogonal grids. In the new definition of the matrix, a correction term is appended and the mixed derivative is approximated by averaging. Furthermore, the numerical scheme is more stable and efficient to handle the convective dominated flows which, as it is well known, is not a trivial task to deal with. The resulting version of the IMM, by its flexibility, not only makes it possible to solve the fluid flow equations in curvilinear configurations, but it is also easily adaptable to the most recent and gravitational high resolution schemes for conservation law equations. The TVD–IMM is then an approach to obtain difference equations at arbitrary mesh point and coupled to an efficient TVD scheme which consists on reformulating the classical Lax–Wendroff scheme in such a way that it takes into account the non-orthogonality of the mesh, and then updating it to be like TVD form by appending suitable curvilinear terms [9,16–18]. The flexibility is a major benefit of this approach.

Numerical investigations of buoyancy-induced convection in cavities that have differentially heated walls are numerous. The thermal flow in enclosed cavities has received a great deal of attention and has emerged as a dominant test case [4–6,11]. The paper by De Vahl Davis and Jones [4] is the most comprehensive study of this problem to date. A key contention, which emerged from their 37 solution analysis, reveals two difficulties: The calculation of heat transfer and the resolution of steep temperature gradients in boundary layers adjacent to the confining walls. The detailed numerical studies have become a benchmark case for developers of numerical methods [5,6,8,11,23].

This paper is devoted to:

- Present a numerical technique that is based on IMM coupled with TVD scheme to solve the incompressible Navier–Stokes equations with heat transfer.
- Show that this TVD–IMM algorithm gives a very good results even at high Rayleigh numbers.
- Show that this technique can be used to solve problems, that of buoyancy driven flow, in arbitrary geometries.

In this work the incompressible Navier–Stokes equations expressed in terms of stream–vorticity variables with the Boussinesq approximation for the buoyancy effect are considered and a numerical method is proposed, the present scheme is basically an improved new scheme to that presented in [18] in terms of flux limiters and computation speed. The nonlinear TVD–IMM solver handles sharp gradient regions very well, shows little numerical diffusion, produces no ripples, is able, among other things, to produce the main characteristics of buoyancy driven flow and the resulting method is easy to implement.

In the following sections, the governing equations are introduced. After a detailed description of the IMM method, we present the numerical scheme where the equations are discretized. The applicability of the proposed formulation and the accuracy of the numerical scheme are evaluated by solving test cases available in the literature and by comparing the solutions to the standard benchmarks data.

## 2. Mathematical model

The governing equations for a two-dimensional incompressible unsteady, laminar natural convection flow, with density variation only in the body force term, according to the Boussinesq approximation for the buoyancy effect, can be expressed in primitive variables as

*Continuity*:

$$\frac{\partial u}{\partial x}+\frac{\partial v}{\partial y}=0, \tag{1}$$

*Momentum*:

$$\frac{\partial u}{\partial t}+\frac{\partial u^2}{\partial x}+\frac{\partial uv}{\partial y}=-\frac{1}{\rho}\frac{\partial p}{\partial x}+v\left(\frac{\partial^2 u}{\partial x^2}+\frac{\partial^2 u}{\partial y^2}\right), \tag{2}$$

$$\frac{\partial v}{\partial t}+\frac{\partial uv}{\partial x}+\frac{\partial v^2}{\partial y}=-\frac{1}{\rho}\frac{\partial p}{\partial y}+v\left(\frac{\partial^2 v}{\partial x^2}+\frac{\partial^2 v}{\partial y^2}\right)+g\beta(T-T_{\mathrm{ref}}), \tag{3}$$

*Energy*:

$$\frac{\partial T}{\partial t}+\frac{\partial uT}{\partial x}+\frac{\partial vT}{\partial y}=k\Delta T. \tag{4}$$

In an attempt to reduce the large differences in the order of magnitude that may occur between terms in the field equations, the lengths and velocities are dimensionalized by the characteristic length scale $L$ and by the ratio of thermal diffusivity $k$ to $L$, respectively. Dimensionless temperature $\theta$ is defined as $(T-T_{\mathrm{ref}})/(T_{\mathrm{h}}-T_{\mathrm{c}})$. $T_{\mathrm{h}}$ and $T_{\mathrm{c}}$ are the hot wall and the cold wall temperature, respectively, and the reference temperature is $T_{\mathrm{ref}}=(T_{\mathrm{h}}-T_{\mathrm{c}})/2$. The pressure $P$ and the time are dimensionalized by $\rho kv/L^2$ and $L^2/k$, respectively. The Prandtl number is defined as $Pr=v/k$, Rayleigh number is defined as $Ra=(g\beta L^3(T_{\mathrm{h}}-T_{\mathrm{c}}))/vk$. Here, $g$ is the acceleration resulting from gravity, $\beta$ is the thermal expansion coefficient and $v$ is the kinematic viscosity.

The vorticity $\omega$, kinematically defined as

$$\omega=\nabla\times\mathbf{u},\quad \mathbf{u}=(u,v)\text{ is the vector velocity}, \tag{5}$$

is introduced in the governing equations to eliminate the pressure as solution variable. Taking the curl of the momentum equations (2) and (3) eliminates any gradient field. Applying Eq. (1), the vorticity transport reduces to

*Vorticity*:

$$\frac{\partial \omega}{\partial t}+\frac{\partial u\omega}{\partial x}+\frac{\partial v\omega}{\partial y}=Pr\,\Delta\omega+Ra\,Pr\frac{\partial\theta}{\partial x}. \tag{6}$$

The stream function $\psi$, and hence the velocity $\mathbf{u}$, is then evaluated from the vorticity via the kinematic equation which leads to the following equations:

*Stream function*:

$$-\Delta\psi=\omega, \tag{7}$$

*Velocity*:

$$u=\frac{\partial\psi}{\partial y},\quad v=-\frac{\partial\psi}{\partial x}, \tag{8}$$

*Energy*:

$$\frac{\partial\theta}{\partial t}+\frac{\partial u\theta}{\partial x}+\frac{\partial v\theta}{\partial y}=\Delta\theta. \tag{9}$$

The vorticity equation (6) and the temperature equation (9) should be supplemented with appropriate initial and boundary conditions. As for the elliptic stream equation (7), a boundary conditions should be added.

There are several advantages of using the stream–vorticity formulation for natural convection system. The pressure does not explicitly appear and the elliptic pressure equation takes much longer than kinematic equation (7) to achieve iteration convergence, because of the difference in boundary conditions. Moreover, the continuity equation is identically satisfied. Finally, the stream–vorticity form can predict time-accurate heat transfer problems.

## 3. Discretization method

As a prelude to developing the numerical scheme, it is convenient to describe how any differential operator and any constitutive equation are to be handled. It has to be known that the IMM is a technique to obtain difference equations by assuming a polynomial combination of any physical quantity $\phi$ by some nodal values in the neighborhood of a mesh point $P$:

$$\phi(x) = \sum_{k=0}^{n} C_k^p P_k(x). \tag{10}$$

The polynomial shape functions $(P_k)_k$ turn out to be extremely useful and $(C_k^p)_k$ are the related fitted coefficients.

The differential coefficients of the physical quantity at the mesh point $P$ are obtained by differentiating Eq. (10)

$$\frac{\partial \phi}{\partial x_j} = \sum_{k=0}^{n} C_k^p \frac{\partial P_k}{\partial x_j}. \tag{11}$$

Differential equation (11) can be written in a matrix form as follows:

$$D(P) = M_D(P) \cdot \Phi(P), \tag{12}$$

where $D(P)$ is a vector of the $n+1$ differential coefficients. Here, the vector $\Phi(P)$ consists of the $n+1$ nodal values of the physical quantity and the matrix $M_D(P)$ is the interpolating matrix in the physical space. Accordingly, any differential equation can be transformed to a difference equation by the help of $M_D(P)$.

There are two distinct approaches to discretizing a domain: structured and unstructured. In the IMM, a structured grid can be viewed as a mapping from a natural space to a physical space. This provides a way of making a convenient transformation between a local, computational space $(\xi, \eta)$ (natural coordinates) and global, physical space $(x, y)$. Fig. 1 shows the geometry in both physical and natural coordinate space.

We define the approximate polynomial equation (10) in the transformed plane. The interpolating matrix $M_D(P)$ in terms of the $\xi_i$ system is obtained as

$$D_\xi(P) = M_{D_\xi} \cdot \Phi(P). \tag{13}$$

The interpolating matrix $M_{D_\xi}$ is assumed to be homogeneous for every mesh point $P$. With the help of the transformation matrix $T_{\xi \to x}$ that is defined as

$$D(P) = T_{\xi \to x} D_\xi(P), \tag{14}$$

the following expression for the interpolating matrix $M_D(P)$ in terms of the $x$ coordinate system is obtained:

$$M_D(P) = T_{\xi \to x} \cdot M_{D_\xi}, \tag{15}$$

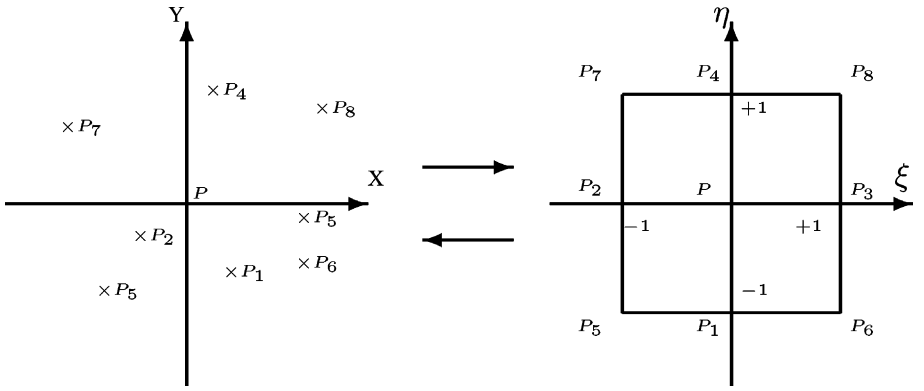


Fig. 1. Coordinate transformation between physical space and natural space.

where the matrix $T_{\xi\to x}$ can be thought of as inducing general curvilinear coordinates in physical space and involves terms such as $x_\xi, x_\eta, x_{\xi\xi}, \ldots$

### 3.1. Typical interpolation

The biquadratic shape functions are used. Thus, for a quantity $\phi$ one can write

$$\phi = c_0 + c_1\xi + c_2\eta + c_3\xi^2 + c_4\eta^2 + c_5\xi\eta + c_6\xi^2\eta + c_7\xi\eta^2 + c_8\xi^2\eta^2. \tag{16}$$

Note that at point $P$, the higher-order mixed derivatives of $\phi$ are equal to zero, except for the lowest-order one $\phi_{\xi\eta} = c_5$. The $\xi$- and $\eta$-derivatives of $\phi$ are given as follows:

$$\begin{pmatrix} \phi_\xi \\ \phi_\eta \\ \phi_{\xi\xi} \\ \phi_{\eta\eta} \\ \phi_{\xi\eta} \end{pmatrix} = \begin{pmatrix} 0 & -\frac{1}{2} & \frac{1}{2} & 0 & 0 \\ -\frac{1}{2} & 0 & 0 & \frac{1}{2} & 0 \\ 0 & 1 & 1 & 0 & 0 \\ 1 & 0 & 0 & 1 & 0 \\ 0 & 0 & 0 & 0 & \frac{1}{4} \end{pmatrix} \begin{pmatrix} \phi_1 - \phi_0 \\ \phi_2 - \phi_0 \\ \phi_3 - \phi_0 \\ \phi_4 - \phi_0 \\ \phi_5 + \phi_8 - \phi_6 - \phi_7 \end{pmatrix}. \tag{17}$$

Here $\phi_i$ $(i = 1, \ldots, 8)$, represents the $\phi$-variable values at point $P$. The derivatives in $(x, y)$ and $(\xi, \eta)$ coordinate systems are related as

$$\begin{pmatrix} \phi_x \\ \phi_y \\ \phi_{xx} \\ \phi_{yy} \\ \phi_{xy} \end{pmatrix} = \begin{pmatrix} \xi_x & \eta_x & 0 & 0 & 0 \\ \xi_y & \eta_y & 0 & 0 & 0 \\ \xi_{xx} & \eta_{xx} & \xi_x^2 & \eta_x^2 & 2\xi_x\eta_x \\ \xi_{yy} & \eta_{yy} & \xi_y^2 & \eta_y^2 & 2\xi_y\eta_y \\ \xi_{xy} & \eta_{xy} & \xi_x\xi_y & \eta_x\eta_y & \xi_x\eta_y + \xi_y\eta_x \end{pmatrix} \begin{pmatrix} \phi_\xi \\ \phi_\eta \\ \phi_{\xi\xi} \\ \phi_{\eta\eta} \\ \phi_{\xi\eta} \end{pmatrix}. \tag{18}$$

Observe that, for the second-order derivatives, the transformation produces a lower-order term in $\phi$ and the approximation of the second derivative will involve nine neighboring points. The combination of Eqs. (17) and (18) gives

$$\begin{pmatrix} \phi_x \\ \phi_y \\ \phi_{xx} \\ \phi_{yy} \\ \phi_{xy} \end{pmatrix} = \underbrace{[\mathrm{IM}] \begin{pmatrix} \phi_1 - \phi_0 \\ \phi_2 - \phi_0 \\ \phi_3 - \phi_0 \\ \phi_4 - \phi_0 \end{pmatrix}}_{\mathrm{I}} + \underbrace{\begin{pmatrix} 0 \\ 0 \\ 2\xi_x\eta_x\phi_m \\ 2\xi_y\eta_y\phi_m \\ (\xi_x\eta_y + \xi_y\eta_x)\phi_m \end{pmatrix}}_{\mathrm{II}}, \tag{19}$$

where the matrix

$$[\mathrm{IM}] = \begin{pmatrix} -\frac{\eta_x}{2} & -\frac{\xi_x}{2} & \frac{\xi_x}{2} & \frac{\eta_x}{2} \\ -\frac{\eta_y}{2} & -\frac{\xi_y}{2} & \frac{\xi_y}{2} & \frac{\eta_y}{2} \\ -\frac{\eta_{xx}}{2}+\eta_x^2 & -\frac{\xi_{xx}}{2}+\xi_x^2 & \frac{\xi_{xx}}{2}+\xi_x^2 & \frac{\eta_{xx}}{2}+\eta_x^2 \\ -\frac{\eta_{yy}}{2}+\eta_y^2 & -\frac{\xi_{yy}}{2}+\xi_y^2 & \frac{\xi_{yy}}{2}+\xi_y^2 & \frac{\eta_{yy}}{2}+\eta_y^2 \\ -\frac{\eta_{xy}}{2}+\eta_x\eta_y & -\frac{\xi_{xy}}{2}+\xi_x\xi_y & \frac{\xi_{xy}}{2}+\xi_x\xi_y & \frac{\eta_{xy}}{2}+\eta_x\eta_y \end{pmatrix} \tag{20}$$

is called the interpolating matrix. The term I in Eq. (19) represents a central approximation of the first- and second-order derivatives and the term II is a correction to the second-order derivatives when the coordinate transformation is non-orthogonal. Moreover, the mixed partial derivative is approximated by averaging using values at the four center points

$$\phi_m = \frac{(\phi_5 - \phi_6 + \phi_8 - \phi_7)}{4}.$$

**Remark.** At each point $P$, represented by the reference number $ij$, the interpolating matrix elements are denoted by $\mathrm{coeff}(i,j,ij)$, where the indices $i,j,ij$ represent, respectively, the mesh point number neighbor of the point $P$ (see Fig. 2), the differential coefficient type ($1 \to \partial/\partial x$, $2 \to \partial/\partial y$, $3 \to \partial^2/\partial x^2$, $4 \to \partial^2/\partial y^2$, $5 \to \partial^2/\partial x y^2$) and the reference of the mesh point $P$. $\phi_{ij}$ is the value of $\phi$ at the mesh point $P$ and $\phi_n$ ($n = 1,\ldots,8$) is the value of $\phi$ at the neighboring point $n$.

From Eq. (19), the differential operator $\partial\phi/\partial x$ can be written as follows:

$$\begin{aligned} \frac{\partial\phi}{\partial x} &= \mathrm{coeff}(1,1,ij)(\phi_1 - \phi(ij)) + \mathrm{coeff}(2,1,ij)(\phi_2 - \phi(ij)) \\ &\quad + \mathrm{coeff}(3,1,ij)(\phi_3 - \phi(ij)) + \mathrm{coeff}(4,1,ij)(\phi_4 - \phi(ij)), \end{aligned} \tag{21}$$

where

$$\mathrm{coeff}(1,1,ij) = -\frac{\eta_x}{2}, \quad \mathrm{coeff}(2,1,ij) = -\frac{\xi_x}{2}, \quad \mathrm{coeff}(3,1,ij) = \frac{\xi_x}{2}, \quad \mathrm{coeff}(4,1,ij) = \frac{\eta_x}{2}.$$

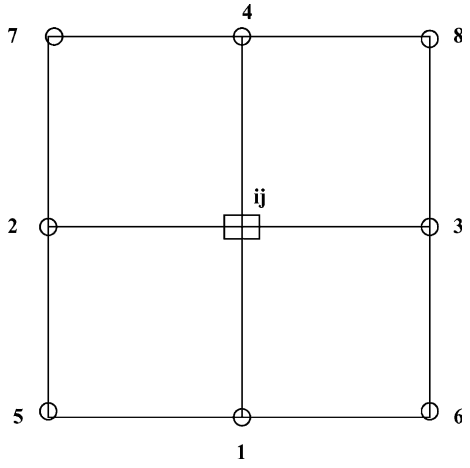


Fig. 2. Mesh point number $(1,\ldots,8)$ neighbor of the point $P$ represented by the reference number $ij$.

The differential operators

$$\left(\frac{\partial\phi}{\partial y},\frac{\partial^2\phi}{\partial x^2},\frac{\partial^2\phi}{\partial y^2},\frac{\partial^2\phi}{\partial xy^2}\right)$$

can be calculated from (19) in the same manner.

## 4. Numerical scheme

We shall first review the Sweby analysis to the Lax–Wendroff scheme and his modification via the flux TVD limiters [7,10,21,22,25]. Then, we describe Davis' interpretation to the Sweby TVD method, as a Lax–Wendoroff scheme plus an upwind weighted artificial dissipation term. Finally, we derive the TVD–IMM approximation to the solution of the natural convection problem.

### 4.1. Review of the TVD limiting

Since the Lax–Wendroff scheme, for the scalar linear conservation law

$$\frac{\partial\omega}{\partial t}+a\frac{\partial\omega}{\partial x}=0 \tag{22}$$

is not TVD, Sweby chooses a particular modification by adding a limiter to the second-order term

$$\omega_j^{n+1}=\omega_j^n-v\left[1+\tfrac{1}{2}(1-v)\left(\Psi(r_j^+)/r_j^+-\Psi(r_{j-1}^+)\right)\right](\omega_j^n-\omega_{j-1}^n). \tag{23}$$

The slope ratio and the CFL number are defined by

$$v=\frac{a\Delta t}{\Delta x},\quad r_j^+=\frac{\omega_j^n-\omega_{j-1}^n}{\omega_{j+1}^n-\omega_j^n},\quad r_j^-=\frac{\omega_{j+1}^n-\omega_j^n}{\omega_j^n-\omega_{j-1}^n}, \tag{24}$$

where $r^+$ is to be used if the waves are right-moving, otherwise $r^-$ is used. The function $\Psi$ is a flux limiter, to be specified. More specifically, the sufficient condition to be TVD is given by

$$0\leqslant\frac{\Psi(r)}{r}\leqslant 2,\quad 0\leqslant\Psi(r)\leqslant 2. \tag{25}$$

Many particular flux limiter functions are well investigated in the literature. The most usual include

$$\text{Superbee}: \quad \Psi(r)=\max(0,\min(1,2r),\min(r,2)),$$

$$\text{Van Leer}: \quad \Psi(r)=\frac{r+|r|}{1+|r|},$$

$$\text{Minmod}: \quad \Psi(r)=\max(0,\min(r,1)).$$

Davis showed that a TVD scheme can be constructed by adding an artificial viscosity-like term to a standard finite difference scheme [3]. If we put the scheme into the form

$$\begin{aligned}\omega_j^{n+1}=\omega_j^n&-\frac{v}{2}(\omega_{j+1}^n-\omega_{j-1}^n)+\frac{v^2}{2}(\omega_{j+1}^n-2\omega_j^n+\omega_{j-1}^n)+\left[K_{j+\frac{1}{2}}^+(r_j^+)+K_{j+\frac{1}{2}}^-(r_{j+1}^-)\right](\omega_{j+1}^n-\omega_j^n)\\&-\left[K_{j-\frac{1}{2}}^+(r_{j-1}^+)+K_{j-\frac{1}{2}}^-(r_j^-)\right](\omega_j^n-\omega_{j-1}^n),\end{aligned} \tag{26}$$

this reduces to Sweby's scheme, where the upstream weighted artificial dissipation terms are as follows:

$$K^{+}_{j+\frac{1}{2}} = \begin{cases} \frac{v}{2}(1-v)(1-\Psi(r^{+}_{j})) & \text{if } a > 0, \\ 0 & \text{if } a \leqslant 0, \end{cases} \tag{27}$$

$$K^{-}_{j+\frac{1}{2}} = \begin{cases} 0 & \text{if } a \geqslant 0, \\ \frac{v}{2}(1+v)(\Psi(r^{-}_{j+1})-1) & \text{if } a < 0. \end{cases} \tag{28}$$

### 4.2. TVD–IMM algorithm

As indicated in Section 1, we begin by designing the time stepping scheme which is a further development of that already discussed in a previous work [18]. The methodology developed here is based on a geometrical version of the nonlinear Lax–Wendroff scheme and the operator splitting procedure. In the following, we outline the main principles upon which the algorithm is built.

#### 4.2.1. Vorticity approximation

*Prediction step*. The differential coefficients in the Cartesian space are estimated at each mesh point. The differential equation is then directly transformed to a difference equation. The one-step Lax–Wendroff scheme for the two-dimensional vorticity-convection equation is written in the IMM form as

$$\bar{\omega}^{n}_{ij} = \omega^{n}_{ij} - \Delta t\delta_x(u\omega)^n - \Delta t\delta_y(v\omega)^n + \frac{\Delta t^2}{2}u\left[\delta_{xx}(u\omega)^n + \delta_{xy}(v\omega)^n\right] + \frac{\Delta t^2}{2}v\left[\delta_{yy}(v\omega)^n + \delta_{yx}(u\omega)^n\right], \tag{29}$$

where the IMM's difference operators are defined by

$$\begin{aligned}\delta_x\phi = {} & \mathrm{coeff}(1,1,ij)(\phi(\mathrm{neigh}(1,ij)) - \phi(ij)) + \mathrm{coeff}(2,1,ij)(\phi(\mathrm{neigh}(2,ij)) - \phi(ij)) \\ & + \mathrm{coeff}(3,1,ij)(\phi(\mathrm{neigh}(3,ij)) - \phi(ij)) + \mathrm{coeff}(4,1,ij)(\phi(\mathrm{neigh}(4,ij)) - \phi(ij)),\end{aligned} \tag{30}$$

$$\begin{aligned}\delta_{xx}\phi = {} & \mathrm{coeff}(1,3,ij)(\phi(\mathrm{neigh}(1,ij)) - \phi(ij)) + \mathrm{coeff}(2,3,ij)(\phi(\mathrm{neigh}(2,ij)) - \phi(ij)) \\ & + \mathrm{coeff}(3,3,ij)(\phi(\mathrm{neigh}(3,ij)) - \phi(ij)) + \mathrm{coeff}(4,3,ij)(\phi(\mathrm{neigh}(4,ij)) - \phi(ij)) \\ & + Gx(ij)\phi_m,\end{aligned} \tag{31}$$

$$\begin{aligned}\delta_{xy}\phi = {} & \mathrm{coeff}(1,5,ij)(\phi(\mathrm{neigh}(1,ij)) - \phi(ij)) + \mathrm{coeff}(2,5,ij)(\phi(\mathrm{neigh}(2,ij)) - \phi(ij)) \\ & + \mathrm{coeff}(3,5,ij)(\phi(\mathrm{neigh}(3,ij)) - \phi(ij)) + \mathrm{coeff}(4,5,ij)(\phi(\mathrm{neigh}(4,ij)) - \phi(ij)) \\ & + Gxy(ij)\phi_m.\end{aligned} \tag{32}$$

The symbol $\mathrm{coeff}(.,.,ij)$ represents the differential coefficient in the interpolating matrix at mesh point $ij$. Similarly, operators $\delta_y$ and $\delta_{yy}$ can be determined by (30) and (31) but in the second column of $\mathrm{coeff}(\cdot,\cdot,ij)$ the numbers 1 and 3 are replaced by 2 and 4, respectively. The symbol $\mathrm{Neigh}(n,ij)$ is the reference of point $P_n$ neighbour of mesh point $ij$. The weights $Gx(ij) = 2\xi_x\eta_x$ and $Gxy(ij) = \xi_x\eta_y + \xi_y\eta_x$ as defined in Eq. (19).

*TVD correction*. As the proposed scheme produces spurious wiggles in solutions with steep gradients, according to the class of the governing equations (coupling of the chaining type between the temperature and the vorticity) and regarding to the explicit nature of the scheme that will lead to a component

by component use of an upstream artificial viscosity. The scheme (29) can be updated to TVD form by appending to the right-hand side of Eq. (29) suitable curvilinear terms (for more details see [18]):

$$\begin{aligned}&\left[K^+(rx^+_{i,j})+K^-(rx^-_{i+1,j})\right]\Delta\omega^n_{i+\frac{1}{2},j}-\left[K^+(rx^+_{i-1,j})+K^-(rx^-_{i,j})\right]\Delta\omega^n_{i-\frac{1}{2},j}\\&\quad+\left[K^+(ry^+_{i,j})+K^-(ry^-_{i,j+1})\right]\Delta\omega^n_{i,j+\frac{1}{2}}-\left[K^+(ry^+_{i,j-1})+K^-(ry^-_{i,j})\right]\Delta\omega^n_{i,j-\frac{1}{2}}.\end{aligned}\tag{33}$$

The resulting TVD-correction vorticity value is then given by

$$\begin{aligned}\bar{\bar{\omega}}^n_{ij}=&\bar{\omega}^n_{ij}+\left[K^+(rx^+_{i,j})+K^-(rx^-_{i+1,j})\right]\Delta\omega^n_{i+\frac{1}{2},j}-\left[K^+(rx^+_{i-1,j})+K^-(rx^-_{i,j})\right]\Delta\omega^n_{i-\frac{1}{2},j}\\&+\left[K^+(ry^+_{i,j})+K^-(ry^-_{i,j+1})\right]\Delta\omega^n_{i,j+\frac{1}{2}}-\left[K^+(ry^+_{i,j-1})+K^-(ry^-_{i,j})\right]\Delta\omega^n_{i,j-\frac{1}{2}},\end{aligned}\tag{34}$$

where

$$K^+(rx^+_{i,j})=\begin{cases}(cp1+cp2)(1-\Psi(rx^+_{i,j})) & \text{if } u^n_{ij}>0,\\ 0 & \text{if } u^n_{ij}<0,\end{cases}\tag{35}$$

with

$$\begin{aligned}cp1&=\Delta tu^n_{ij}(\mathrm{coeff}(3,1,ij)-0.5\Delta tu^n_{ij}\mathrm{coeff}(3,3,ij)),\\cp2&=\Delta tv^n_{ij}(\mathrm{coeff}(3,2,ij)-0.5\Delta tv^n_{ij}\mathrm{coeff}(3,4,ij))\end{aligned}\tag{36}$$

and

$$K^-(rx^-_{i+1,j})=\begin{cases}(\bar{c}p1+\bar{c}p2)(1-\Psi(rx^-_{i+1,j})) & \text{if } u^n_{ij}<0,\\ 0 & \text{if } u^n_{ij}>0,\end{cases}\tag{37}$$

with

$$\begin{aligned}\bar{c}p1&=-\Delta tu^n_{ij}(\mathrm{coeff}(3,1,ij)+0.5\Delta tu^n_{ij}\mathrm{coeff}(3,3,ij)),\\\bar{c}p2&=-\Delta tv^n_{ij}(\mathrm{coeff}(3,2,ij)+0.5\Delta tv^n_{ij}\mathrm{coeff}(3,4,ij)).\end{aligned}\tag{38}$$

It is to be noticed that the artificial viscosity terms $K^{\pm}$ depend upon the interpolating matrix coefficients. The input to the limiter is the ratio of the consecutive gradients

$$rx^+_{i,j}=\frac{\Delta\omega^n_{i-\frac{1}{2},j}}{\Delta\omega^n_{i+\frac{1}{2},j}},\quad rx^-_{i,j}=\frac{\Delta\omega^n_{i+\frac{1}{2},j}}{\Delta\omega^n_{i-\frac{1}{2},j}},\tag{39}$$

where

$$\Delta\omega^n_{i-\frac{1}{2},j}=\omega^n_{i,j}-\omega^n_{i-1,j},\quad \Delta\omega^n_{i,j-\frac{1}{2}}=\omega^n_{i,j}-\omega^n_{i,j-1}.\tag{40}$$

*Correction step*. Upon solution of convective stage, the new vorticity field is obtained from Eq. (34) by appending the diffusion term, thus the vorticity value at the time step $n+1$ is given by

$$\begin{aligned}\omega^{n+1}_{ij}=&\bar{\bar{\omega}}^n_{ij}+\left[K^+(rx^+_{i,j})+K^-(rx^-_{i+1,j})\right]\Delta\omega^n_{i+\frac{1}{2},j}-\left[K^+(rx^+_{i-1,j})+K^-(rx^-_{i,j})\right]\Delta\omega^n_{i-\frac{1}{2},j}\\&+\left[K^+(ry^+_{i,j})+K^-(ry^-_{i,j+1})\right]\Delta\omega^n_{i,j+\frac{1}{2}}-\left[K^+(ry^+_{i,j-1})+K^-(ry^-_{i,j})\right]\Delta\omega^n_{i,j-\frac{1}{2}}\\&+\Delta t\,Pr\left[\delta_{xx}\omega^n+\delta_{yy}\omega^n\right]+Ra\,Pr\,\delta_x\theta.\end{aligned}\tag{41}$$

*4.2.2. Energy approximation*

The time energy discretization is established in a similar way:

*Prediction step.*

$$\bar{\theta}_{ij}^{n} = \theta_{ij}^{n} - \Delta t\delta_x(u\theta)^n - \Delta t\delta_y(v\theta)^n + \frac{\Delta t^2}{2}u\left[\delta_{xx}(u\theta)^n + \delta_{xy}(v\theta)^n\right] + \frac{\Delta t^2}{2}v\left[\delta_{yy}(v\theta)^n + \delta_{yx}(u\theta)^n\right]. \tag{42}$$

*Correction step.*

$$\begin{aligned}\theta_{ij}^{n+1} = \bar{\theta}_{ij}^{n} &+ \left[K^+(rx_{i,j}^+) + K^-(rx_{i+1,j}^-)\right]\Delta\theta_{i+\frac{1}{2},j}^{n} - \left[K^+(rx_{i-1,j}^+) + K^-(rx_{i,j}^-)\right]\Delta\theta_{i-\frac{1}{2},j}^{n} \\ &+ \left[K^+(ry_{i,j}^+) + K^-(ry_{i,j+1}^-)\right]\Delta\theta_{i,j+\frac{1}{2}}^{n} - \left[K^+(ry_{i,j-1}^+) + K^-(ry_{i,j}^-)\right]\Delta\theta_{i,j-\frac{1}{2}}^{n} + \Delta t\delta_{xx}\theta^n.\end{aligned} \tag{43}$$

*4.2.3. Stream function approximation*

For stream equation, an IMM discretization is adopted such that generalized differences are used to approximate the original partial differential equation. The resolution is based on the successive over-relaxation, widely used for this kind of elliptic equation. The velocity components $u_{ij}^{n+1}$ and $v_{ij}^{n+1}$ can be computed from the stream function $\psi$ as

$$u_{ij}^{n+1} = \delta_y\psi^{n+1}, \quad v_{ij}^{n+1} = -\delta_x\psi^{n+1}. \tag{44}$$

## 5. Results and discussion

In order to demonstrate the validity of the TVD–IMM scheme and to check its accuracy, we have computed different solutions of the buoyancy driven cavity flow. The flow is steady inside an upright ($\beta = 90°$) and inclined ($\beta = 45°$) square cavity with insulated top and bottom walls and with side walls maintained at constant but different temperatures (see Fig. 3). This classical problem has become a standard benchmark for assessing the performance of algorithms to solve the heat transfer equations [4–6,8,23].

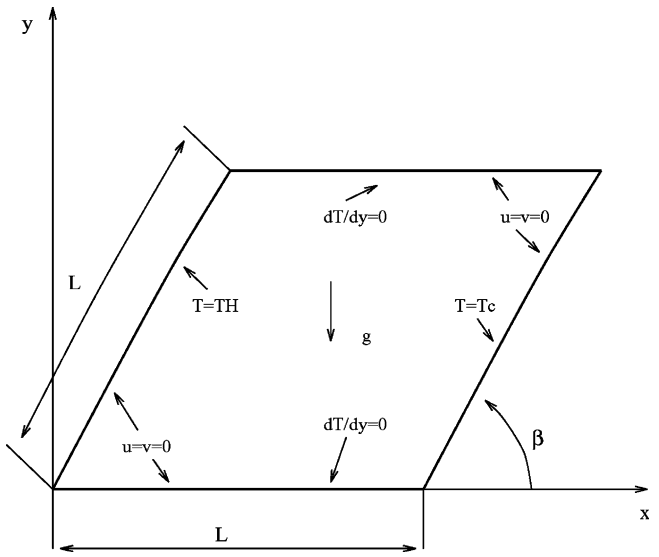


Fig. 3. Geometry and boundary conditions for the buoyancy-driven cavity problem.

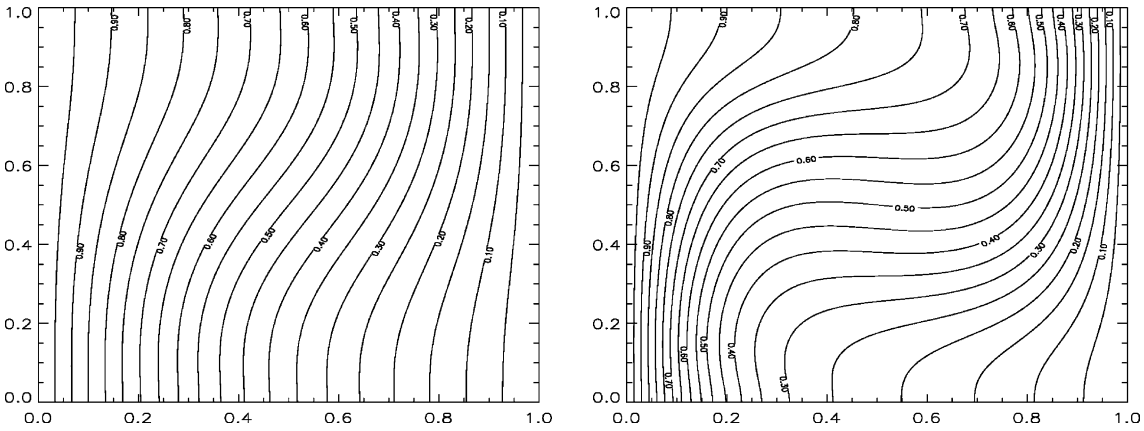

Fig. 4. Contour map of temperature $T$ for $Pr = 0.71$ and Rayleigh numbers $Ra = 10^3$, $Ra = 10^4$.

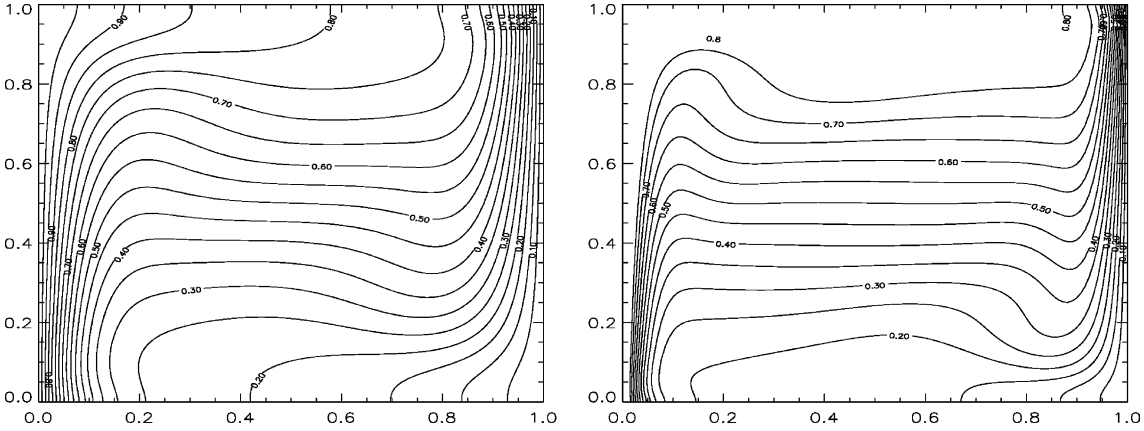

Fig. 5. Contour map of temperature $T$ for $Pr = 0.71$ and Rayleigh numbers $Ra = 10^5$, $Ra = 10^6$.

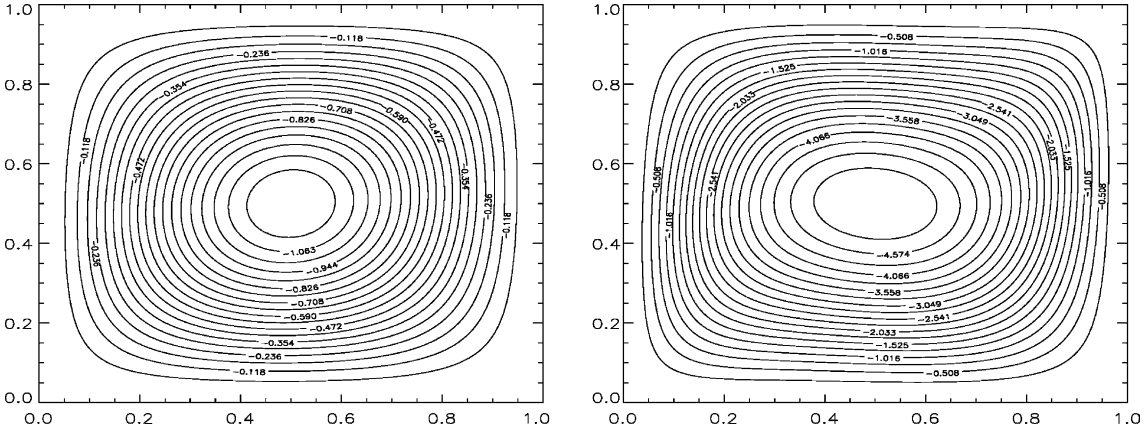

Fig. 6. Contour map of stream function $\psi$ for $Pr = 0.71$ and Rayleigh numbers $Ra = 10^3$, $Ra = 10^4$.

### 5.1. Buoyancy-driven cavity

*Square cavity case*. As a preliminary test to investigate the behaviour of the flow structure of air ($Pr = 0.71$), we have computed the different solutions of the above described problem for four values of the Rayleigh number $Ra = 10^3$, $10^4$, $10^5$ and $10^6$. The most accurate benchmark solutions of this case were produced by De Vahl Davis and Jones [4,5]. Gresho et al. [8] and Winters [23].

*Evolution of flow structure*. For Rayleigh number $10^3$ and $10^4$, the flow shows a single clockwise cell in the enclosure (see Fig. 6). At Rayleigh number $10^5$, a secondary recirculation eddies starts to form and a significant horizontal temperature gradient is increased near the cold and hot walls (see Fig. 7(a)). As the Rayleigh number continue to rise, the wall boundary layers become thinner and more pronounced (see Figs. 7 and 10(b)). The structure of the flow near the corners of the cavity is emphasized (see Fig. 8(b)).

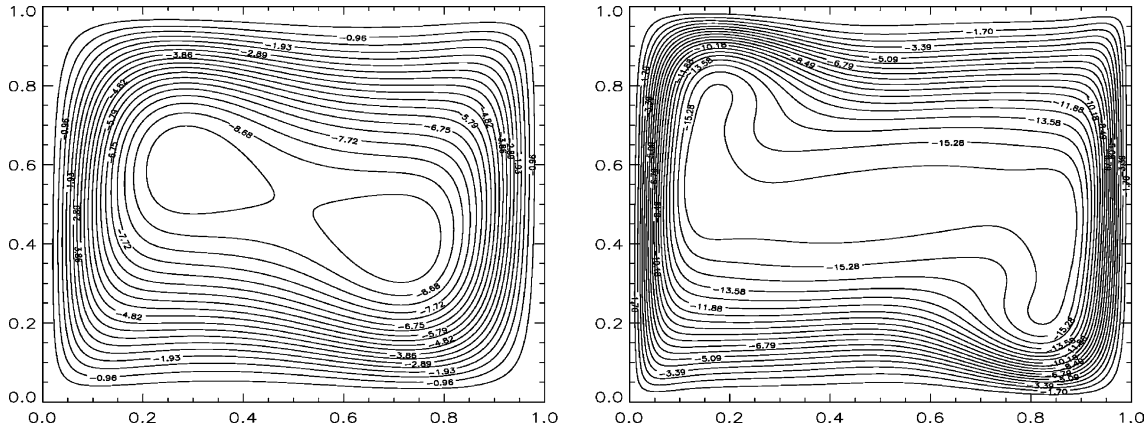

Fig. 7. Contour map of stream function $\psi$ for $Pr = 0.71$ and Rayleigh numbers $Ra = 10^5$, $Ra = 10^6$.

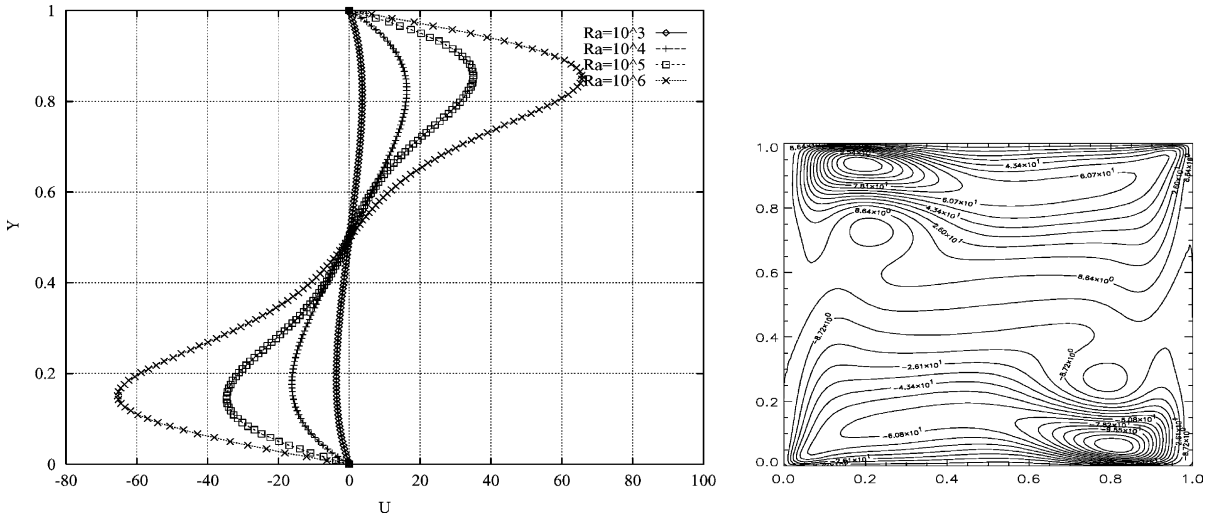


Fig. 8. Horizontal velocity for different values of Rayleigh number and $U$-velocity contour for $Ra = 10^6$.

*Validation of the numerical method*. Stream lines, vorticity lines and isotherms predicted by TVD–IMM on the $(120 \times 120)$ uniformly spaced grid and using Suberbee flux limiter are presented in Figs. 4–7, 9 and 10. Horizontal velocities on the vertical plane at $x = 0.5$ and vertical velocities on the horizontal plane at $y = 0.5$ are plotted in Figs. 8 and 11(a). The results of the present simulations accurately reproduced the distinctive characteristics of the flow field known from previous studies.

Data from the TVD–IMM experiment are compiled in Tables 1–4. We note by $\psi_{\text{mid}}$ the stream function at the mid point of the cavity; $u_{\max}$ the maximum horizontal velocity on the vertical plain at $x = 0.5$, together with its location; $v_{\max}$ the maximum vertical velocity on the horizontal plain at $y = 0.5$, together with its location. Tables 1–3 compare $\psi_{\text{mid}}$, $u_{\max}$, $v_{\max}$ from the present study with other numerical results. From these tables, it can be seen that the present result agrees particularly well with the result from [4,5,8,23].

*Inclined cavity*. This test has been motivated by some industrial applications. It has been proved that the heat transfer, in heat exchangers, is enhanced when the tube is optimally inclined [15]. The purpose of this test is to show the ability of IMM to predict the natural-convection flow in non-orthogonal grids. The following test is proposed by Demirdzic et al. [6] as benchmark reference for $Ra = 10^6$ with $Pr = 0.71$ and $Ra = 10^6$ with $Pr = 0.1$.

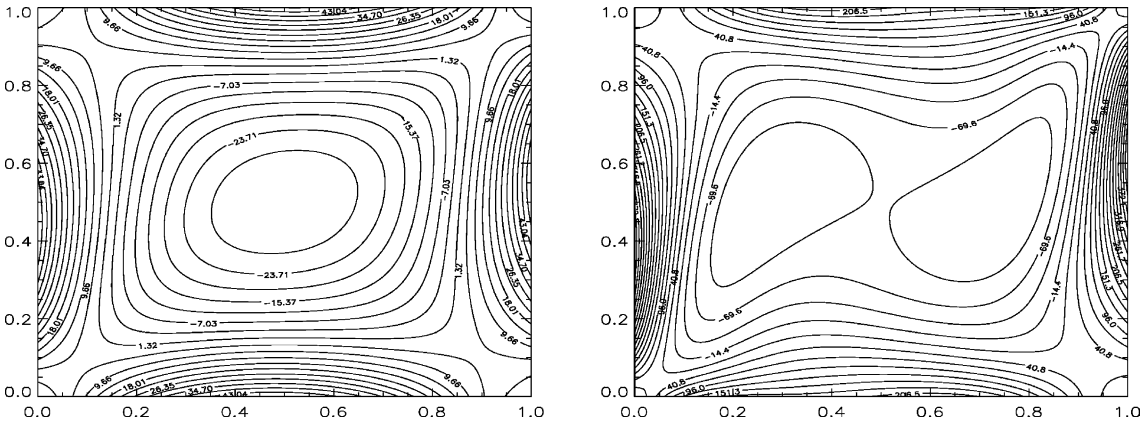

Fig. 9. Contour map of vorticity $\omega$ for $Pr = 0.71$ and Rayleigh numbers $Ra = 10^3$, $Ra = 10^4$.

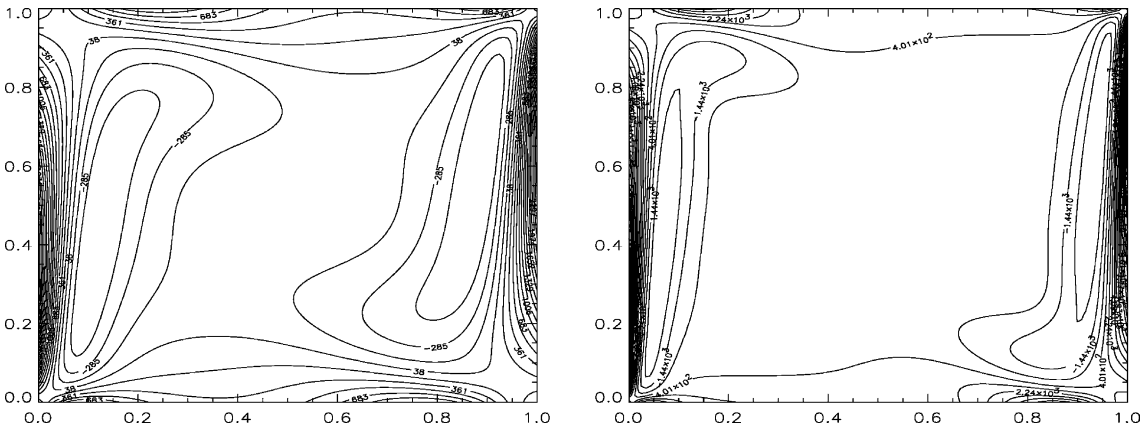

Fig. 10. Contour map of vorticity $\omega$ for $Pr = 0.71$ and Rayleigh numbers $Ra = 10^5$, $Ra = 10^6$.

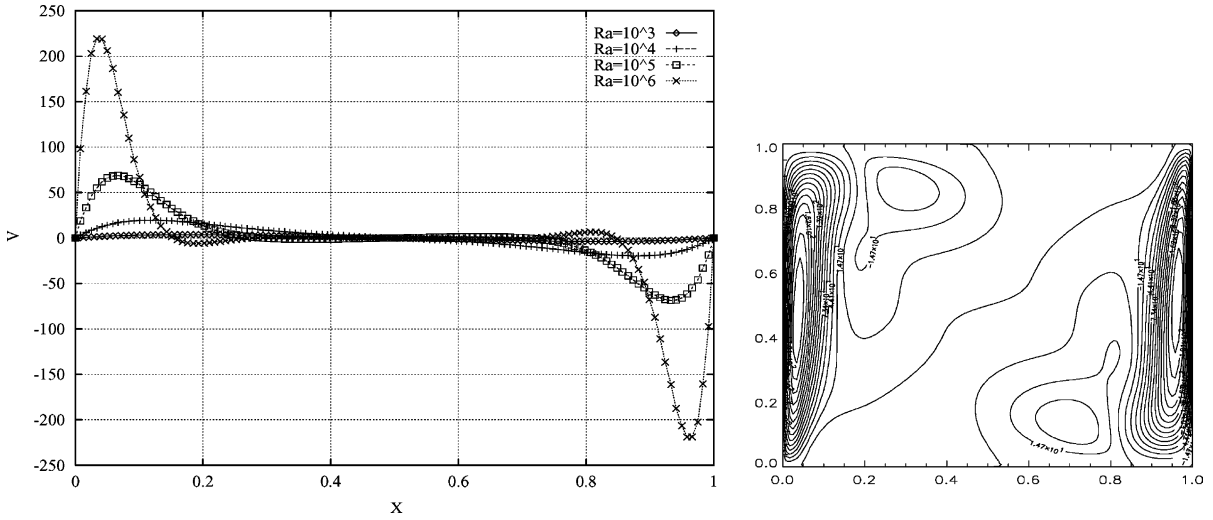


Fig. 11. Vertical velocity for different values of Rayleigh number and $V$-velocity contour for $Ra = 10^6$.

Table 1
Minimum and maximum stream function values in vortex centres and their position for Rayleigh number $Ra = 10^3$

| | De Vahl's results | Gresho's results | Winters' results | TVD–IMM's results |
|---|---|---|---|---|
| $Ra = 10^3$ and $\beta = 90°$ | | | | |
| $\lvert\psi_{mid}\rvert$ | 1.174 | – | – | 1.180 |
| $u_{max}$ | 3.634 | 3.656 | 3.64 | 3.663 |
| $y$ | 0.813 | 0.812 | 0.81 | 0.815 |
| $v_{max}$ | 3.679 | 3.704 | 3.69 | 3.716 |
| $x$ | 0.179 | 0.166 | 0.1 | 0.176 |

Table 2
Minimum and maximum stream function values in vortex centres and their position for Rayleigh number $Ra = 10^4$

| | De Vahl's results | Gresho's results | Winters' results | TVD–IMM's results |
|---|---|---|---|---|
| $Ra = 10^4$ and $\beta = 90°$ | | | | |
| $\lvert\psi_{mid}\rvert$ | 5.098 | – | – | 5.0824 |
| $u_{max}$ | 16.182 | 16.193 | 16.2 | 16.2184 |
| $y$ | 0.823 | 0.822 | 0.82 | 0.824 |
| $v_{max}$ | 19.509 | 19.675 | 19.7 | 19.686 |
| $x$ | 0.120 | 0.120 | 0.1187 | 0.118 |

Table 3
Minimum and maximum stream function values in vortex centres and their position for Rayleigh number $Ra = 10^5$

| | De Vahl's results | Gresho's results | Winters' results | TVD–IMM's results |
|---|---|---|---|---|
| $Ra = 10^5$ and $\beta = 90°$ | | | | |
| $\lvert\psi_{mid}\rvert$ | 9.142 | – | – | 9.344 |
| $u_{max}$ | 34.81 | 34.62 | 34.8 | 35.03 |
| $y$ | 0.855 | 0.856 | 0.86 | 0.857 |
| $v_{max}$ | 68.22 | 68.896 | 68.6 | 68.651 |
| $x$ | 0.066 | 0.0663 | 0.066 | 0.0671 |
| $\lvert\psi_{max}\rvert$ | 9.644 | 9.6206 | 9.307 | 9.644 |

Table 4
Minimum and maximum stream function values in vortex centres and their position for Rayleigh number $Ra = 10^6$

| | De Vahl's results | Gresho's results | Winters' results | TVD–IMM's results |
|---|---|---|---|---|
| $Ra = 10^6$ and $\beta = 90°$ | | | | |
| $\lvert\psi_{mid}\rvert$ | 16.53 | – | – | 16.88 |
| $u_{max}$ | 65.33 | 64.593 | 63.9 | 65.64 |
| $y$ | 0.851 | 0.888 | 0.85 | 0.849 |
| $v_{max}$ | 216.75 | 220.64 | 222. | 219.145 |
| $x$ | 0.0387 | 0.0337 | 0.039 | 0.035 |
| $\lvert\psi_{max}\rvert$ | 16.961 | 16.707 | 16.71 | 16.972 |

*Evolution of flow structure*. Contrary to the case of horizontal cavities, where a stagnant region develops in the center of the layer as a consequence of a vanishing buoyancy force at the core, in inclined cavities, a buoyant production of vorticity exists in the core of the cavity owing to the presence of cross-stream

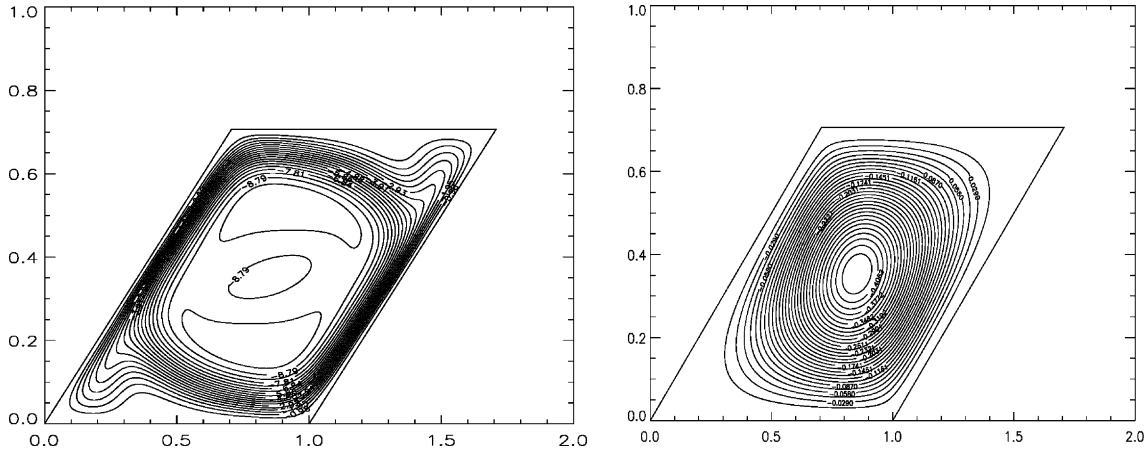

Fig. 12. Contour map of stream function for $Pr = 0.1$, $Ra = 10^6$ and $Pr = 0.71$, $Ra = 10^6$ with $\beta = 45°$.

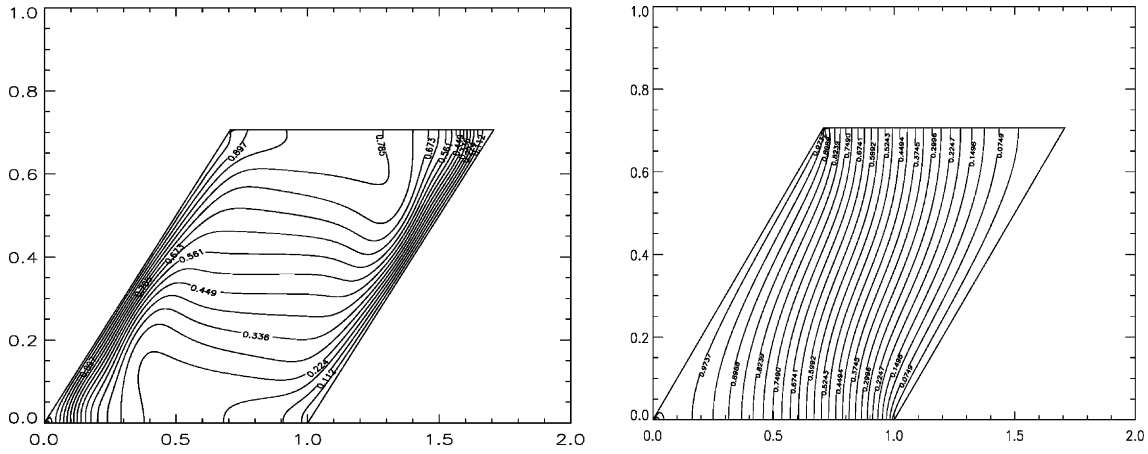

Fig. 13. Contour maps of temperature for $Pr = 0.1$, $Ra = 10^6$ and $Pr = 0.71$, $Ra = 10^6$ with $\beta = 45°$.

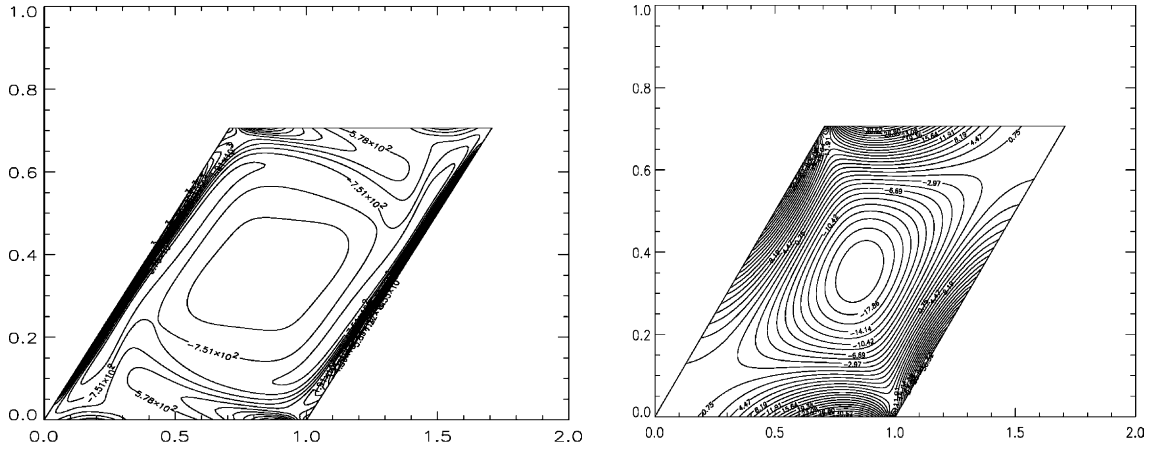

Fig. 14. Contour map of vorticity for $Pr = 0.1$, $Ra = 10^6$ and $Pr = 0.71$, $Ra = 10^6$ with $\beta = 45°$.

Table 5
Maximum stream function value and position as predicted for Rayleigh number $Ra = 10^6$

| | Demirdzics' results | TVD–IMM's results |
|---|---|---|
| $Ra = 10^6$ and $\beta = 45°$ | | |
| $\lvert\psi_{max}\rvert$ | 7.705E − 08 | 9.1809197E − 07 |
| $y_{max}$ | 0.7026 | 0.6950 |
| $x_{max}$ | 1.271738 | 1.275000 |

temperature difference and the $y$ component of gravity. The thermo convective movement produces an isotherm line deviation (see Fig. 13). As shown in Figs. 12 and 14, two flow regions may be distinguished: the core region, containing a parallel clockwise flow and the end regions near the closing walls, where the parallel flow turns around. Qualitatively, the results obtained by the TVD–IMM approach are in good agreement with Demirdzic's solutions [6].

*Validation of the numerical method.* In this study, some of flow quantities obtained by Demirdzic et al. [6] are used to validate our numerical calculations. In particular, the maximum stream function value $\psi_{max}$ is compared in Table 5 for Rayleigh number $10^6$ and Prandtl number 0.1. It should be noted that due to the different ways of non-dimensionalization between Demirdzic et al. [6] and the authors, the equivalent $\psi_{max}$ in Table 5 is the one from Demirdzic multiplied by $10^{-3}$. It can be seen that the present results generally agree well with those of Demirdzic et al. [6].

## 6. Concluding remarks

In this paper we have presented a numerical algorithm for the resolution of Navier–Stokes equations of a Boussinesq fluid enclosed in two-dimensional upright and inclined square cavity. An original high-resolution second-order accurate scheme was proposed. The method has been applied to study the standard heat transfer problems. Numerical predictions are compared with those of previous benchmark data of the overall cavity flow. In summary, the benchmarks prove that the numerical method proposed is robust and accurate even in the limiting cases of high Rayleigh numbers.

## References

[1] A. Bejan, A.N. Rossie, Natural convection in a horizontal duct connecting two fluid reservoirs, Trans. ASME, J. Heat Transfer 103 (1981) 108–113.
[2] B.E. Boyack, D.W. Kearney, Heat transfer by laminar natural convection in low aspect ratio cavities, Technical Report, 72-HT-2, ASME, 1972.
[3] F. Davis, TVD finite difference schemes and artificial viscosity, Icase Report, no. 84-20, 1984.
[4] G. De Vahl Davis, I.P. Jones, Natural convection in a square cavity: a comparison exercise, Int. J. Numer. Methods Fluids 3 (1983) 227–248.
[5] G. De Vahl Davis, Natural convection on air in a square cavity: a benchmark numerical solution, Int. J. Numer. Methods Fluids 3 (1983) 249–264.
[6] I. Demirdzic, Z. Lilek, M. Peric, Fluid flow and heat transfer test problems for non-orthogonal grids: benchmark solutions, Int. J. Numer. Methods Fluids 15 (1992) 329–354.
[7] J.B. Goodman, R.J. Leveque, A geometric approach to high resolution TVD schemes, Icase Report no. 55–84, 1984.
[8] P.M. Gresho, C.D. Upson, R.L. Lee, Finite element simulations of thermally induced convection in an enclosed cavity, Lawrence Livermore Laboratory Report UCID-18602, 1980.
[9] L. Hanich, M. Louaked, Interpolating matrix method prediction of flow with heat transfer, in: 8th International Symposium on Computational Fluid Dynamics Conference, Bremen, Germany, 1999.
[10] A. Harten, On a class of high resolution total variation stable finite difference schemes, SIAM J. Numer. Anal. 21 (1984) 1–23.
[11] M. Hortmann, M. Peric, G. Scheuerer, Finte volume multigrid prediction of laminar natural convection: benchmark solutions, Int. J. Numer. Methods Fluids 11 (1990) 189–207.
[12] S.S. Koshizuka et al., Interpolating matrix method: a finite difference method for arbitrary arrangement of mesh points, J. Comput. Phys. 75 (1988) 444–468.
[13] W.E. Langlois, Buoyancy driven flows in crystal growth melts, Ann. Rew. Fluid Mech. 17 (1985) 191–215.
[14] P. Le Quere, T. Alziary De Roquefort, Computation of natural convection in two-dimensional cavities with Chebyshev polynomials, J. Comput. Phys. 57 (1985) 210–228.
[15] G.S.H. Lock, J. Fu, Natural convection in the inclined cranked thermosyphon, J. Heat Transfer 115 (1993) 167–172.
[16] M. Louaked, L. Hanich, K.D. Nguyen, An improved TVD scheme to resolve the Navier–Stokes equations in stream–vorticity formulation by the interpolating matrix method, in: W.H. Hui, J.R. Yue-Kuen Kwok, Chasnov (Eds.), First Asian Computational Fluid Dynamics Conference, vol. 2, Hong Kong University of Science and Technology, 1995, pp. 421–426.
[17] M. Louaked, L. Hanich, K.D. Nguyen, High resolution of the 2D Navier–Stokes equations by the interpolating matrix method, in: K.W. Morton, M.J. Baines (Eds.), Numerical Methods for Fluid Dynamics, Oxford University Press, Oxford, 1996, pp. 457–464.
[18] M. Louaked, L. Hanich, K.D. Nguyen, An efficient finite difference technique for computing incompressible viscous flows, Int. J. Numer. Methods Fluids 25 (1997) 1057–1082.
[19] L.A.B. Pilkington, Proc. R. Soc. Lond. A 314 (1969) 1.
[20] M. Ravi, M. Henkes, J. Hoogendoorn, On the high-Rayleigh-number structure of steady laminar natural-convection flow in a square enclosure, J. Fluid Mech. 262 (1994) 325–352.
[21] P.L. Roe, Generalized formulation of TVD Lax–Wendroff schemes, Icase Report, no. 84-53, 1984.
[22] P. Sweby, High resolution schemes using flux limiters for hyperbolic conservation laws, SIAM J. Numer. Anal. (1984) 995–1011.
[23] K.H. Winters, A numerical study of natural convection in a square cavity, United Kingdom Atomic Energy Authority, AERE-R9747, 1980.
[24] A.W. Woods, S.J. Lintz, Natural convection and dispersion in a tilted fracture, J. Fluid Mech. 237 (1992) 57.
[25] H. Yee, Construction of explicit and implicit symmetric TVD schemes and their applications, J. Comput. Phys. 68 (1987) 151–179.